Light scattering from quantum spin fluctuations in R_2CuO_4 (R = La, Nd, Sm)

P. E. Sulewski, P. A. Fleury, and K. B. Lyons
AT&T Bell Laboratories, Murray Hill, New Jersey 07974

S-W. Cheong and Z. Fisk
Los Alamos National Laboratory, Los Alamos, New Mexico 87545
(Received 17 July 1989)

Raman spectra reveal spin fluctuation scattering over the energy range 0–8000 cm^{-1} (0–1 eV) in single crystal La_2CuO_4 (T phase), Nd_2CuO_4, and Sm_2CuO_4 (T' phase). From the B_{1g} symmetry spectra, values of the exchange parameter J for these crystals are determined to be 1030±50, 871±50, and 888±50 cm^{-1}, respectively. All three materials also exhibit broad spectral features of A_{1g} and B_{2g} symmetry, which are forbidden within the classical spin-pair excitation model, but allowed by quantum fluctuations. The line shapes for spectra of all three symmetries agree with recent model calculations for the planar calculations for the planar quantum antiferromagnet. While the spectra for crystals with the T' structure are nearly identical, subtle differences from the spectra of La_2CuO_4 (T structure) indicate a sensitivity to the structure outside of the CuO_2 planes.

I. INTRODUCTION

Recently, a comparison of our inelastic-light-scattering spectra with a theoretical calculation[1] of nearest neighbor spin-pair scattering for the spin-$\frac{1}{2}$ planar Heisenberg antiferromagnet has dramatically demonstrated that quantum fluctuations are responsible for the anomalously large linewidth observed[2] for B_{1g} symmetry in La_2CuO_4. In addition, it was argued that the quantum fluctuations could permit next-nearest-neighbor scattering processes, forbidden in the pure Néel (classical) ground state, of A_{1g} and B_{2g} symmetry. The observation of this A_{1g} scattering intensity in La_2CuO_4 was previously noted.[1,3]

In La_2CuO_4 the observed spectral weight in the A_{1g} feature is of the same order of magnitude as the B_{1g} feature, contrary to naive expectations. Contributions to the spin-pair scattering cross section involving the influence of the atoms outside of the CuO_2 planes might explain the observed magnitude of the A_{1g} feature. In such a case, one may argue that the spectra might be sensitive to the out-of-plane structure. In this paper, we present spectra from three single crystals: La_2CuO_4, Nd_2CuO_4, and Sm_2CuO_4, which have a different out-of-plane structure. For La_2CuO_4 (T), the Cu has octahedral coordination to the oxygen, while in Nd_2CuO_4 and Sm_2CuO_4 (T') the coordination is square planar[4] (see Fig. 1).

II. EXPERIMENTAL DETAILS

The La_2CuO_4 crystal, grown from a pure CuO flux, is the same crystal used in previous works[1,3] and has a measured Néel temperature of 265 K. The Nd_2CuO_4 and Sm_2CuO_4 single crystals were grown from a CuO flux, as has been previously described.[5] For the Nd_2CuO_4, $T_N \sim 245$ K. Susceptibility and neutron scattering determinations of T_N for Sm_2CuO_4 are precluded by its large temperature-dependent paramagnetism and the large neutron absorption cross section of Sm. Since each of the as-grown crystals exhibited at least one highly reflecting face, free of residual flux, no polishing was necessary, and all spectra were taken from as-grown surfaces. The basal plane dimensions of the La_2CuO_4, Nd_2CuO_4, and Sm_2CuO_4 crystals were 8×10, 3×2, and 4×6.5 mm^2, respectively.

The spectra were obtained with 20 mW from an Ar ion laser focused to a line 0.1×1.5 mm^2 on the samples at room temperature. Three excitation wavelengths—5145, 4880, and 4579 Å—were used to probe the resonance behavior of the features of interest. The laser power was determined with a Coherent Model 210 power meter.

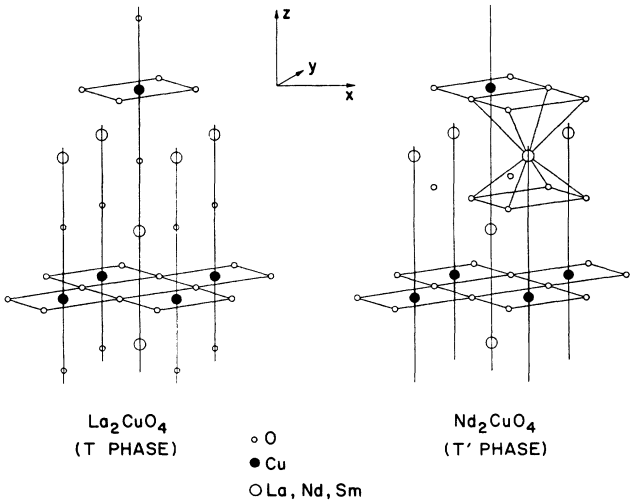

FIG. 1. Comparison of the T and T' crystal structures. For the T structure, the Cu ions are surrounded by oxygen octahedra, while for the T' structure, the Cu ions are fourfold coordinated to the oxygen ions in the plane.

The scattered light was collected at right angles to the incident beam with f/4 optics and passed through a Spex Triplemate spectrometer to a liquid-nitrogen-cooled charge-coupled-device (CCD) camera. The spectra have all been calibrated to a standard lamp to correct for the response of the spectrometer and detector, so that the spectra at different excitation frequencies may be directly compared.

The crystal structures for the T and T' phases, shown in Fig. 1, both exhibit two-dimensional (2D) CuO_2 sheets. In the T phase, the Cu ions are sixfold coordinated to the surrounding oxygens, which enclose the Cu ions in an octahedral cage, as shown in Fig. 1. The La ion is ninefold coordinated to the surrounding oxygens, four of which lie in the CuO_2 plane below the La, four of which are the apical oxygens from the four surrounding octahedra, and the apical oxygen is located in the octahedron directly above it.

In the T' phase the rare-earth ions remain above (and below) the centers of the CuO_2 squares. However, the coordination of the oxygens to the rare-earth ions becomes eightfold by moving the apical oxygens further from the plane, to lie midway between the two nearest CuO_2 sheets and directly above and below the in-plane oxygens. This displacement of the apical oxygens destroys the octahedral coordination at the Cu sites, resulting in a square planar coordination. The rare-earth ion thus sits in the center of a tetragonal cage of oxygens.

In order to discuss the various symmetry components of the Raman tensor, the axes along the planar Cu—O bonds are defined as x and y. The x' and y' axes are defined by a 45° rotation from the xy axes. With the incident and scattered light both polarized along the y axis (yy), the spectrum contains the A_{1g} and B_{1g} symmetry components. The yx spectrum reveals the B_{2g} component. After a simple 45° rotation of the crystal, the polarized scattering ($y'y'$) gives the sum of the A_{1g} and B_{2g} scattering, while the depolarized scattering ($y'x'$) gives the B_{1g} component. Any contribution from surface fluorescence will appear in all of these symmetry combinations. In the case of Nd_2CuO_4 and Sm_2CuO_4, this contribution appears to be less than 5% of the B_{1g} peak value, while it is somewhat larger for La_2CuO_4. The fluorescence background may be removed from the A_{1g} by subtracting the yx spectrum from the $y'y'$ spectrum, to obtain the pure A_{1g} component. The background cannot be so unambiguously removed from the B_{1g} and B_{2g} components, however, and the spectra presented here include this contribution to the intensity, which therefore contributes to the uncertainty in the scattering cross section.

III. DATA AND DISCUSSION

A. B_{1g} features

The most prominent feature in the Raman spectra of the insulating cuprates[2,6] is the B_{1g} spin pair mode, which is shown in Figs. 2(a)–2(c). This B_{1g} scattering is well-described[7] by the effective interaction Hamiltonian:[8]

$$H_R = C \sum_{(ij)} (\mathbf{E}_{\rm inc} \cdot \boldsymbol{\sigma}_{ij})(\mathbf{E}_{\rm sc} \cdot \boldsymbol{\sigma}_{ij}) \mathbf{S}_i \cdot \mathbf{S}_j, \quad (1)$$

where $\mathbf{E}_{\rm inc}$ and $\mathbf{E}_{\rm sc}$ are electric field vectors for the incident and scattered photons, and $\boldsymbol{\sigma}_{ij}$ is a unit vector connecting spin sites i and j. The matrix elements and other details of the excited-state exchange[9] determining H_R are contained in the prefactor C.

The spectra shown in Figs. 2(a)–2(c) all peak near 3000 cm^{-1}, and exhibit widths [full width at half maximum (FWHM)] of about 1200 cm^{-1}. In addition, the curves have similar asymmetries, with greater spectral weight appearing on the high-frequency side of the peaks. Since the theoretical calculation[1] can provide only values for the frequency moments, or equivalently the cumulants, of the lineshape $I(\omega)$, the cumulants of the curves in Figs. 2(a)–2(c) have been extracted using

$$M_1 = \int \omega I(\omega) d\omega / I_T, \quad (2)$$

$$(M_n)^n = \int (\omega - M_1)^n I(\omega) d\omega / I_T, \quad (3)$$

for $n > 1$, where

$$I_T = \int I(\omega) d\omega. \quad (4)$$

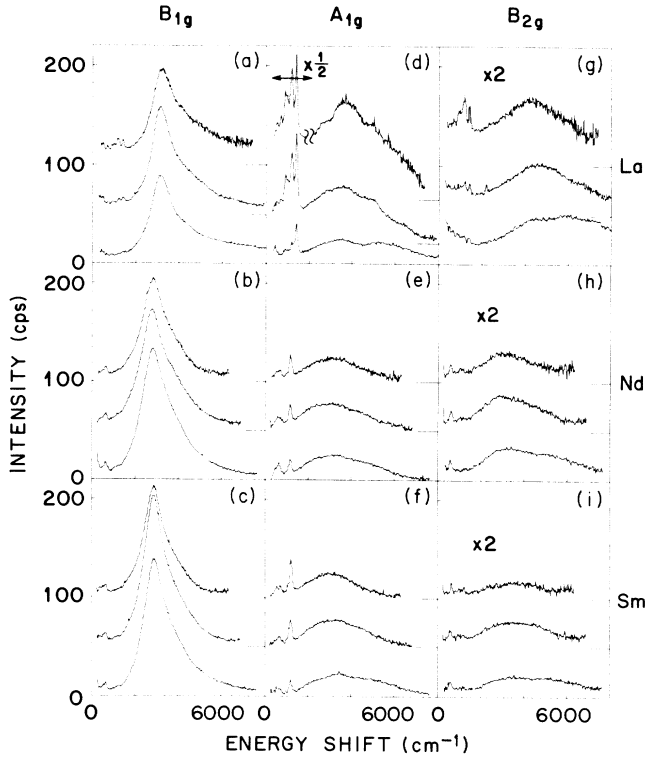

FIG. 2. Raman spectra of various symmetries for several incident laser wavelengths. The baselines are indicated at the right for the upper two spectra in each figure part, which are shifted upward for clarity. The curves are ordered according to their laser excitation wavelength, λ_L: 5145 Å (top), 4880 Å (middle), and 4579 Å (bottom, unshifted). Spectra have been separated according to their symmetry: (a)–(c) B_{1g}, (d)–(f) A_{1g}, and (g)–(i) B_{2g}. For each symmetry, spectra are shown for each of the three compounds: (a), (d), (g) La_2CuO_4; (b), (e), (h) Nd_2CuO_4; (c), (f), (i) Sm_2CuO_4. The A_{1g} and B_{1g} spectra are plotted on the same scale, for ease of comparison, while the B_{2g} spectra are multiplied by a factor of 2. Note also that the low frequency portion of the 5145 Å spectrum in (d) is reduced by a factor of 2.

TABLE I. Values of the cumulants of the B_{1g} spin-pair mode for La_2CuO_4, Nd_2CuO_4, and Sm_2CuO_4 at several laser excitation wavelengths.

Sample	λ_L (Å)	ω_p (cm^{-1})	M_1 (cm^{-1})	M_2 (cm^{-1})	M_3 (cm^{-1})	M_2/M_1
	5145	3210 ± 10	3760 ± 50	850 ± 50	840 ± 100	0.23
La_2CuO_4	4880	3130	3650	940	830	0.26
	4579	3133	3700	1050	990	0.28
	5145	2806	3014	722	460	0.24
Nd_2CuO_4	4880	2760	3110	860	675	0.28
	4579	2800	3240	910	780	0.28
	5145	2858	3044	693	460	0.23
Sm_2CuO_4	4880	2859	3167	794	633	0.25
	4579	2897	3330	920	820	0.28
Theory			3.6 J	0.8 J	1.0 J	0.23

The values of peak position and the various cumulants are tabulated in Table I. In calculating the cumulants, the fluorescence background is subtracted by assuming a linear form and setting the spectral intensity to zero at the high- and low-frequency limits of the mode. For any particular sample, the variations among the peak and cumulant values for different laser wavelengths found in Table I provide limits on the influence of this background subtraction.

From the cumulants in Table I, values for the exchange parameter J may be extracted, given the theoretical prediction[1] that $M_1/J = 3.58 \pm 0.06$. Averaging the values obtained for different laser wavelengths, we find J to be 1030 ± 50 cm^{-1}, 871 ± 50 cm^{-1}, and 888 ± 50 cm^{-1}, for La_2CuO_4, Nd_2CuO_4, and Sm_2CuO_4, respectively. The value of J for La_2CuO_4 compares well with the value of $J = 1080 \pm 40$ cm^{-1} obtained from recent inelastic neutron scattering experiments.[10]

The value of the second cumulant, M_2, provides a dramatic verification of the dominant role of quantum fluctuations, and supports the validity of Ising series expansion methods.[1] In particular, the observed ratios of M_2/M_1, as given in the last column of Table I, are close to the theoretical value of 0.23 ± 0.02. Conventional spin-wave theory,[8] which ignores quantum fluctuations, predicts the much smaller ratio $M_2/M_1 = 0.11$. The narrower width predicted by spin wave theory is indeed observed in the isomorphic K_2NiF_4 spin-1 system.[7] The third cumulant, although more sensitive to the experimental background subtraction procedure, is in quite reasonable agreement with the theoretical prediction of $M_3/M_1 = 0.27$, for all three samples. Spin wave theory predicts $M_3/M_1 = 0.06$..

Returning to the exchange parameter J, Table II compares J values derived from Fig. 2 with the Cu-O distances of La_2CuO_4,[11] Nd_2CuO_4,[12] Sm_2CuO_4,[12] and $Ba_2YCu_3O_6$.[13] Within the three-band Hubbard model, the dependence of J on the Cu-O distance can be qualitatively understood. For weak exchange, with $t_0 \ll U$, ε_p,[14]

$$J = \frac{4t_0^4}{\varepsilon_p^2 U} + \frac{4t_0^4}{2\varepsilon_p^3}, \tag{5}$$

where t_0 is the Cu to O hopping rate, ε_p is the one-electron oxygen on-site energy, and U is the on-site Coulomb repulsion at the Cu ion. Although the accepted values[15] of $t_0 \sim 1.3$ eV and $\varepsilon_p \sim 3.6$ eV for La_2CuO_4 violate the assumptions under which Eq. (5) is valid, qualitatively at least, it predicts that as the Cu-O distance is reduced, t_0 increases, leading to an increase in J, as observed (see Table II). Comparing the J values derived for La_2CuO_4, $Ba_2YCu_3O_6$, and $Bi_2Sr_2Ca_{1-x}Y_xCu_2O_{8+y}$ also yields an increasing J with decreasing Cu-O distance,[16] although the variation of ε_p due to crystal-field effects for the very different structures may play an important role. More realistic calculations are needed to provide a more reliable estimate of the dependence of J on the Cu-O distance.

Examining superexchange antiferromagnets with weak exchange,[17] specifically X_2MF_4 (X=K,Rb,Tl; M=Mn,Co,Ni), shows that the Hubbard model provides an adequate description of the dependence of J on the M-F separation, when J is in the range of applicability of Eq. (5). Approximating the distance dependence of the p-d overlap by a power law,[18] and ignoring any change in U or ε_p, leads to $J \sim d^{-n}$ with $n = 14$. This compares favorably with the experimental value[17] $n \sim 12$. For the cuprates, we find $0 \lesssim n \lesssim 4$. We attribute this disagreement to the fact that the exchange is too strong for Eq. (5) to apply to the cuprates. However, the success of the Hubbard model for the fluorides suggests that calculations in a limit more appropriate to the cuprates might yield a useful description in that case as well.

B. A_{1g} and B_{2g} features

As mentioned, classical theory[8] predicts only B_{1g} scattering intensity for the planar nearest-neighbor

TABLE II. Comparison of the exchange parameter J, derived from the spectra for various compounds, with the Cu-O distance.

Sample	Cu-O distance (Å)	J (cm^{-1})
La_2CuO_4	1.907	1030
Nd_2CuO_4	1.970	871
Sm_2CuO_4	1.955	888
$Ba_2YCu_3O_6$	1.941	792

Heisenberg antiferromagnet. Accounting for quantum fluctuations in the ground state leads to additional allowed scattering in the A_{1g} and B_{2g} symmetries. The spectra observed in these symmetries are shown in Figs. 2 (d)–2(i), for the three compounds. Both features are much broader than the B_{1g} modes of Figs. 2(a)–2(c). The much sharper structure in the A_{1g} spectra near 1500 cm^{-1} has been attributed to two-phonon scattering[19] and will not be discussed further here. For the purposes of the discussion that follows, these phonons are subtracted off by extrapolating the intensity at a frequency above the phonons linearly to zero at zero frequency. By varying the frequency at which the extrapolation begins, an estimate of the error incurred may be obtained. The fluorescence background that is present in the B_{2g} data is estimated and subtracted in the same manner as in the B_{1g} case. The resulting error estimates are larger in the B_{2g} case, however, since the spectral weight is much smaller in these features than in the B_{1g} mode.

In the classical Néel ground state, the spins on nearest-neighbor (NN) Cu sites are aligned antiparallel. The diagonal-next-neighbor (DNN) sites are on the same sublattice, and therefore have aligned spins. In the spin-$\frac{1}{2}$ case, quantum fluctuations lead to a 30% probability that DNN spins will be antiparallel, which allows a spin-pair excitation by Eq. (1), with σ_{ij} being a unit vector connecting a given site to a DNN site. This new DNN term gives rise to both A_{1g} and B_{2g} scattering. Ising series-expansion calculations predict[1] that these features are broader than the B_{1g} scattering with $M_1 \approx 3.5J$, $M_2 \approx 1.2J$ for A_{1g}, and $M_1 \approx 3.9J$, $M_2 \approx 1.1J$ for B_{2g}. Within the same model, the ratio of the B_{2g} to A_{1g} integrated intensities is calculated to be ~ 0.4. The cumulants calculated from the A_{1g} and B_{2g} data are displayed in Table III, as ratios to the J, which is obtained from the B_{1g} spectrum at each laser frequency. In addition, the ratios of the total integrated intensities of B_{1g} to A_{1g} and B_{2g} to A_{1g} are indicated. From the table, the cumulants predicted by the Ising series-expansion are seen to agree to within $\sim 20\%$ with the experiment. The ratios of the B_{2g} to A_{1g} integrated intensities lie somewhat below the expected value of ~ 0.4. However, since the integrated intensity of the fluorescence background may be comparable to that of the B_{2g} feature, the experimental uncertainties in this ratio are large.

Although the Ising series-expansion calculation[1] gives a reasonable agreement with the observed A_{1g} and B_{2g} moments, it makes no predictions regarding the relative magnitude of the conventional nearest-neighbor (B_{1g}) and the quantum-fluctuation-allowed DNN (A_{1g} and B_{2g}) processes. We may, however, estimate these relative magnitudes as follows. Because Eq. (1) has the formal appearance of an exchange term, it might seem that the simplest way to produce the DNN coupling required for the A_{1g} process is to perform the NN spin exchange twice. From this viewpoint, one expects this higher-order process to have a cross section orders of magnitude smaller than the NN one. However, Fig. 2(a) and 2(d) show that experimentally the two are comparable in La_2CuO_4, with a ratio of the B_{1g} to A_{1g} spectral intensities varying from 0.4 to 1.5, depending on excitation wavelength. Thus, either the A_{1g} and B_{2g} spectra are not due to spin-pair excitations, or this expectation is overly simplistic. It has been suggested that the A_{1g} and B_{2g} features may arise from charge transfer rather than spin-pair excitations.[20] We expect the relevant electronic energies, and therefore the spectral peak positions, to change substantially among the three compounds. However, the observed frequencies for the A_{1g} and B_{2g} features remain approximately the same for all three materials. That is, they scale very well with J, as determined from the B_{1g} feature, which provides strong evidence of their magnetic rather than charge transfer origin.

The Raman cross sections for the NN and DNN processes are calculated from matrix elements of the exchange operator, $V_{ex} = e^2/r_{ij}$. These same matrix elements determine the ground-state exchange J. The small DNN ground-state exchange thus appears to imply a small DNN to NN intensity ratio. In calculating the Raman cross sections, however, the exchange matrix elements are weighted by dipole matrix elements and energy denominators which may emphasize intermediate states coupling equally well to NN and DNN sites. Obvious

TABLE III. Ratios of the cumulants and integrated intensities of the A_{1g}, B_{1g}, and B_{2g} scattering for La_2CuO_4, Nd_2CuO_4, and Sm_2CuO_4, at several laser excitation wavelengths.

		A_{1g}		B_{2g}		I_T	
Sample	λ_L(Å)	M_1/J	M_2/M_1	M_1/J	M_2/M_1	B_{1g}/A_{1g}	B_{2g}/A_{1g}
	5145	3.7	0.38	4.1	0.22	0.39	0.13
La_2CuO_4	4880	3.6	0.39	4.7	0.25	0.84	0.24
	4579	4.2	0.39	5.1	0.23	1.5	0.37
	5145	3.7	0.34	3.9	0.21	2.6	0.27
Nd_2CuO_4	4880	3.8	0.38	4.0	0.25	2.3	0.31
	4579	3.9	0.37	4.6	0.30	2.8	0.45
	5145	3.6	0.33	4.1	0.23	2.6	0.15
Sm_2CuO_4	4880	3.9	0.35	4.1	0.24	2.8	0.24
	4579	4.2	0.35	4.6	0.29	3.1	0.27
Theory		3.5	0.34	3.9	0.28		~ 0.4

candidates considered for these intermediate states are electronic excitations (i) of the La (Nd,Sm) ions, (ii) of the out-of-plane oxygens, and (iii) within the CuO_2 plane. The evidence presented indicates that (iii) and possibly (ii) are realized.

Although some variation is observed in comparing spectra of the T and T' structure samples, it is far less than expected for a mechanism involving (i). The spectra in Fig. 2 show that while the ratio of B_{1g} to A_{1g} integrated intensities for La_2CuO_4 varies from 0.4 to 1.5, this ratio varies between 2.3 and 2.8 for Nd_2CuO_4 and 2.6 and 3.1 for Sm_2CuO_4. In addition, the resonance behavior of the A_{1g} mode changes, as seen in Figs. 2(d)–2(f). While for La_2CuO_4 the A_{1g} features weaken as the laser excitation frequency increases, these features remain relatively constant for Nd_2CuO_4 and Sm_2CuO_4. Although the resonant enhancements in La_2CuO_4 appear consistent with electronic structure calculations,[21] which indicate the presence of unoccupied bands of La character 2 eV above the Fermi energy, similar calculations[22] for Nd_2CuO_4 find that the Nd bands are shifted upward by 2 eV relative to the position of the La bands in La_2CuO_4. Such a large change in the electronic energies would result in much weaker spin-fluctuation scattering in Nd_2CuO_4, contrary to the observations.

Within the CuO_2 plane, the E_u charge transfer mode,[20] which places a hole on the four oxygens not surrounding a Cu site, couples equally to the NN and DNN Cu ions. Changes in the charge transfer gap[23] between La_2CuO_4 and Nd_2CuO_4, which appear at approximately 1.5 eV, may provide an explanation of the decreased DNN coupling in the T' materials. While La_2CuO_4 evidences a "soft gap," the leading edge of the Nd_2CuO_4 gap exhibits a very sharp structure, perhaps signaling the formation of a Cu-O exciton. The formation of an exciton, binding the hole more strongly to the Cu ion in the T' structure, could explain why the DNN coupling is weaker than the NN coupling for these materials. Although the in-plane oxygen E_u charge transfer thus seems a likely candidate for the dominant resonant state, contributions from other states might account for the differences among the three samples. For example, the similarities between Nd_2CuO_4 and Sm_2CuO_4 spectra argue for some involvement of mechanism (ii).

Whatever the microscopic details of the intermediate state, two general facts can be invoked to explain the observed discrepant ratios of the NN to DNN coupling in the ground state and in the Raman cross section: (1) The different symmetries of the interaction Hamiltonian V for the Raman matrix element and the superexchange imply that the virtual transitions will couple to different intermediate states. (2) The presence of the incident photon energy in the energy denominators may enhance the contribution of the various intermediate states to the Raman cross section compared with their appearance in the ground-state superexchange calculation. Encouraged by the success of cluster calculations[24] in describing the La_2CuO_4 system, we believe that the identification of the relevant intermediate states and a calculation of the resonance behavior of the various symmetry Raman cross sections lie within the grasp of theory.

IV. CONCLUSIONS

Inelastic-light-scattering spectra from La_2CuO_4, Nd_2CuO_4, and Sm_2CuO_4 all exhibit pronounced spin-fluctuation scattering of the expected B_{1g} symmetry, from which values of the microscopic Cu-Cu exchange parameter J have been determined. The values lie in the 1000 cm^{-1} range and show a weak decrease with increasing Cu-O distance. The line shapes, absolute intensities, and resonance behavior of the B_{1g} modes for all three compounds are quite similar.

The classically forbidden, but quantum allowed, A_{1g} and B_{2g} diagonal spin-pair spectra for the three materials exhibit subtle differences in absolute intensities and resonance enhancement which correlate with structural differences between the T and T' phases. These changes reflect the sensitivity of the Raman cross section for these modes to the details of the out-of-plane structure. It is hoped that a microscopic understanding of these Raman cross sections will aid in constructing a fuller picture of charge transfer and doping behavior as the antiferromagnetic systems are moved toward the superconducting regime.

ACKNOWLEDGMENTS

We have benefited from many helpful discussions with P. B. Littlewood, L. F. Mattheiss, A. Millis, K. M. Rabe, M. Schluter, R. R. P. Singh, and C. M. Varma. We also thank H. L. Carter for technical assistance.

[1]R. R. P. Singh, P. A. Fleury, K. B. Lyons, and P. E. Sulewski, Phys. Rev. Lett. **62**, 2736 (1989).
[2]K. B. Lyons, P. A. Fleury, L. F. Schneemeyer, and J. V. Waszczak, Phys. Rev. Lett. **60**, 732 (1988).
[3]K. B. Lyons, P. E. Sulewski, P. A. Fleury, H. L. Carter, A. S. Cooper, G. P. Espinosa, Z. Fisk, and S-W. Cheong, Phys. Rev. B **39**, 9693 (1989).
[4]Hk. Muller-Buschbaum and W. Wollschlager, Z. Anorg. Allg. Chem. **414**, 76 (1975).
[5]S-W. Cheong and Z. Fisk (unpublished).
[6]K. B. Lyons, P. A. Fleury, J. P. Remeika, A. S. Cooper, and T. J. Negran, Phys. Rev. B **37**, 2353 (1988).
[7]P. A. Fleury and H. J. Guggenheim, Phys. Rev. Lett. **24**, 1346 (1970).
[8]J. B. Parkinson, J. Phys. C **2**, 2012 (1969).
[9]P. A. Fleury and R. Loudon, Phys. Rev. **166**, 514 (1968).
[10]G. Aeppli, S. M. Hayden, H. A. Mook, Z. Fisk, S-W. Cheong, D. Rytz, J. P. Remeika, G. P. Espinosa, and A. S. Cooper,

Phys. Rev. Lett. **62**, 2052 (1989).
[11]B. Grande, Hk. Muller-Buschbaum, and M. Schweizer, Z. Anorg Allg. Chem. **428**, 120 (1977).
[12]Landolt-Bornstein, *Magnetic and Other Properties of Oxides and Related Compounds*, Vol. 4 of *Group III: Crystal and Solid State Physics*, edited by K.-H. Hellwege and A. M. Hellwege (Springer-Verlag, New York 1970), p. 204.
[13]D. W. Murphy, S. A. Sunshine, P. K. Gallagher, H. M. O'Bryan, R. J. Cava, B. Batlogg, R. B. van Dover, L. F. Schneemeyer, and S. M. Zahurak, in *Chemistry of High-Temperature Superconductors*, ACS Symp. Ser. No. 351, edited by D. L. Nelson, M. S. Whittingham, and T. F. George (ACS, Washington, D.C., 1987), pp. 181–191.
[14]F. C. Zhang and T. M. Rice, Phys. Rev. B **37**, 3759 (1988).
[15]M. S. Hybertsen, M. Schluter, and N. E. Christensen, Phys. Rev. B **39**, 9028 (1989).
[16]S. Sugai, in *Mechanisms of High Temperature Superconductivity*, edited by H. Kamimura and A. Oshiyama (Springer-Verlag, New York, 1989), p. 207.
[17]L. J. de Jongh and R. Block, Physica **79B**, 568 (1975).
[18]W. A. Harrison, *Electronic Structure and the Properties of Solids* (W. H. Freeman, San Francisco, 1980).
[19]S. Sugai, S. Shamoto, and M. Sato, Phys. Rev. B **38**, 6436 (1988).
[20]P. B. Littlewood, C. M. Varma, S. Schmitt-Rink, and E. Abrahams, Phys. Rev. B **39**, 12 371 (1989).
[21]L. F. Mattheiss, Phys. Rev. Lett. **58**, 1028 (1987).
[22]L. F. Mattheiss (unpublished).
[23]S. Tajima, H. Ishii, T. Nakahashi, T. Takagi, S. Uchida, M. Seki, S. Suga, Y. Hidaka, M. Suzuki, T. Murakami, K. Oka, and H. Unoki, J. Opt. Soc. Am. B **6**, 475 (1989).
[24]E. B. Stechel and D. R. Jennison, Phys. Rev. B **38**, 8873 (1988).